On the laboratory generation of two-dimensional, progressive, surface waves of nearly permanent form on deep water

By DIANE M. HENDERSON[1], MATTHEW S. PATTERSON[2]
AND HARVEY SEGUR[3]

[1]William G. Pritchard Fluid Mechanics Laboratory, Department of Mathematics,
Penn State University, University Park, PA 16802, USA

[2]Department of Applied Mathematics, University of Washington, Seattle, WA 98195-2420, USA

[3]Department of Applied Mathematics, University of Colorado, Boulder, CO 80309-0526, USA

Recent experiments by Hammack *et al.* (*J. Fluid Mech.*, vol. 532, 2005, p. 1) on deep-water waves with two-dimensional, periodic surface patterns showed several features, some of which were unsteady. Fuhrman & Madsen (*J. Fluid Mech.*, vol. 559, 2006, p. 391) explained three of these as being the consequence of sinusoidal forcing by the wavemaker array that did not include forced harmonics, either in time or in the direction parallel to the wavemaker. They predicted that neglected third-harmonic terms cause more serious consequences than neglected second-harmonic terms when the generated wavefields have two-dimensional surface patterns. This paper presents experiments that provide strong evidence that their explanation is correct: including the third-harmonic terms in the wavemaker forcing results in wave patterns that propagate with nearly permanent form.

1. Introduction

In this paper we consider the laboratory generation of patterns of surface waves that propagate with nearly permanent form on deep water and that have periodicities in two horizontal dimensions. Such patterns have been observed in experiments by Kimmoun, Branger & Kharif (1999*a*), who generated trains of plane waves that reflected from a wall to create two-dimensional patterns, and by Hammack & Henderson (2003) and Hammack, Henderson & Segur (2005, hereafter referred to as HHS), who used a 32-plunger wavemaker array to generate patterns resulting from the interaction of two trains of plane waves that were symmetric about the direction of pattern propagation. Figure 1 shows a photograph of such a pattern from HHS.

Similar patterns of deep-water surface waves with two-dimensional surface structure have also been generated through bifurcations of one-(horizontal) dimensional wavetrains (Su 1982; Su *et al.* 1982). Other types of two-dimensional surface patterns, termed 'crescent waves' or 'horseshoe' patterns, have been observed in experiments on wind-generated waves by Caulliez, Ricci & Dupont (1998) and Collard & Caulliez (1999). Additional types of wave patterns due to wind have been observed in experiments by Caulliez & Collard (1999). Two-dimensional surface patterns are becoming more and more important in our understanding of deep-water surface waves, so it is important that we be able to generate them with quantitative accuracy and control; this paper is part of that effort.
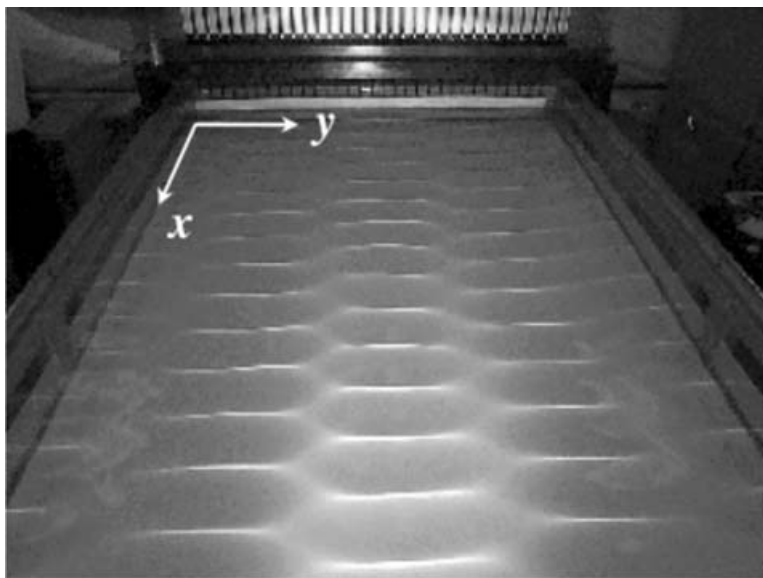
FIGURE 1. A typical bi-periodic pattern of progressive surface waves in deep water.

Here we concentrate on the generation of two-dimensional surface patterns by an array of mechanical wavemakers that are programmed to produce two trains of waves interacting at symmetric, oblique angles from the direction of pattern propagation. HHS catalogued twelve features of their patterns, some of which were unsteady. Examples of the unsteady features were (i) slow modulations, or 'beats' of the wave amplitudes in the x-direction, (ii) curving of crestlines in the y-direction, and (iii) dips and peaks in the crestlines in the y-direction. An explanation for these unsteady features was proposed by Fuhrman & Madsen (2006, hereafter referred to as FM), who conducted numerical experiments using a Boussinesq-type model that is high order in dispersion. They argued that the three unsteady features listed above occurred because the forcing for the wavemaker array used only the first term from the infinite series representing a wave of permanent form.

Even before FM, it was known that when attempting to generate steadily propagating waves with a wavemaker, the omission of higher harmonics from the forcing of the wavemaker could lead to spurious 'free' wave modes that make the wavefield unsteady. See Schäffer & Steenberg (2003) for a review of work that addresses the neglect of second-harmonic terms when generating either planar or non-planar wavefields. The new insight of FM was that for wavefields with two-dimensional surface patterns, the neglect of third-harmonic terms can cause unsteady features that are even more significant than the unsteady features resulting from the neglect of the second-harmonic terms. They argued that it is the neglect of these third-harmonic terms in the Stokes-type solution of two-dimensional surface patterns that caused the unsteady features observed by HHS listed above. FM provided numerical evidence that supports their hypothesis. Herein, we present experimental evidence that verifies their hypothesis for the three unsteady features listed above.

The remainder of the paper proceeds as follows. In §2 we outline the theoretical framework required to discuss the FM predictions. The FM explanation of unsteadiness is independent of additional experimental complications that are caused by the presence of the wavemaker in the laboratory experiments and that could potentially

contribute to unsteadiness. These issues are part of the overall problem of determining a wavemaker forcing that will produce a permanent-form wavefield, which is generally referred to as 'the wavemaker problem'. The wavemaker problem and additional experimental complications are briefly discussed in §3. The particular wavemaker and other experimental apparatus and procedures used herein are described in §4. In §5 we show comparisons of measurements and predictions by FM. The comparison does not include considerations due to the boundary created by the wavemaker, so the agreement shows that FM's results are generic to two-dimensional surface patterns formed by the interaction of trains of plane waves.

2. Aspects of FM's theory

Waves at an air–water interface, such as those shown in the photograph of figure 1, may be described by a classic boundary-value problem for irrotational motion of an incompressible fluid with a free surface (of infinite horizontal extent that neglects the boundary due to the presence of a wavemaker) subject to a gravitational restoring force. (A problem formulation is given in HHS, for example.) Solutions of permanent form for the velocity potential and the surface displacement of the air–water interface may be obtained by expressing these unknowns as a power series expansion in a small parameter, say ϵ. When two trains of plane waves interact at an angle, the surface displacement can be written in the form

$$\eta(x, y, t) = \sum_{j=1}^{\infty} \epsilon^j \eta^{(j)}(x, y, t). \tag{1}$$

See Hsu, Tsuchiya & Silvester (1979), Roberts & Peregrine (1983), Roberts (1983), Roberts & Schwarz (1983), Bryant (1985), Ioualalen (1993), Badulin *et al.* (1995), and HHS for some of the coefficients in this series. For a symmetric surface pattern, the first-order terms are

$$\eta^{(1)}(x, y, t) = \frac{a}{2}\cos(k_x x + k_y y - \omega t) + \frac{a}{2}\cos(k_x x - k_y y - \omega t) = a\cos(k_y y)\cos(k_x - \omega t), \tag{2}$$

in which two waves propagate with wavenumber vectors $\boldsymbol{k} = (k_x, k_y)$ and $\boldsymbol{k} = (k_x, -k_y)$ at angles

$$\theta = \arctan(k_x/k_y) \tag{3}$$

and $-\theta$ to the x-axis. These two waves form a pattern that propagates in the x-direction with an amplitude variation that is trigonometric in y.

To satisfy the kinematic boundary conditions at the sidewalls ($y = 0$ and $y = W$, where W is the width of the tank), necessarily $k_y = n\pi/W$, with $n = 0, 1, 2, \ldots$ being the number of nodal lines. Each nodal line (where the surface displacement vanishes) is a straight line parallel to the x-axis; the wave pattern in figure 1 has four nodal lines: at $y = \frac{1}{8}W, \frac{3}{8}W, \frac{5}{8}W, \frac{7}{8}W$. We note that although the wave pattern in this photograph might look hexagonal, it is not – HHS showed with time series of measurements of the surface displacement there that the nodal regions in figure 1 are straight lines.

To satisfy conservation of mass for an irrotational fluid and the boundary conditions at the air–water interface, the frequency and wavenumber vector in (2) must satisfy the linear dispersion relation,

$$\omega^2 = \sqrt{gk\tanh(kh)}, \qquad k = \sqrt{k_x^2 + k_y^2}, \tag{4}$$

where g is the acceleration due to gravity, h is the water depth, and k is the magnitude of the wavenumber vector.

In the experiments of HHS, the first-order terms in (2), with no higher harmonics, were used to generate patterns like the one shown in figure 1 as described below in §4. FM discussed the effects of HHS's neglecting the second- and third-order terms of the expansion in their wave generation. In particular, FM predicted that one third-order term is responsible for causing the three unsteady features listed in §1. Since our concern here is to test this prediction, we do not write down the second-order terms (equation (4.1) of FM). Instead, the third-order terms, from (4.9) of FM, are

$$\eta^{(3)}(x, y, t) = \frac{a^3 k^2}{2} [b_{11} \cos(k_y y) \cos(k_x x - \omega t) + b_{13} \cos(3k_y y) \cos(k_x x - \omega t)$$
$$+ b_{31} \cos(k_y y) \cos(3k_x x - 3\omega t) + b_{33} \cos(3k_y y) \cos(3k_x x - 3\omega t)]. \quad (5)$$

FM stated that neglecting the terms in (5) in the experimental wave generation leads to the release of spurious free waves of the form

$$\eta_{free}^{(3)}(x, y, t) = -\frac{a^3 k^2}{2} [b_{13} \cos(3k_y y) \cos(k_{13} x - \omega t)$$
$$+ b_{31} \cos(k_y y) \cos(k_{31} x - 3\omega t) + b_{33} \cos(3k_y y) \cos(k_{33} x - 3\omega t)], \quad (6)$$

where $(k_{13}, 3k_y, \omega)$, $(k_{31}, k_y, 3\omega)$, $(k_{33}, 3k_y, 3\omega)$ each satisfy (4). FM proposed that the first term in (6) is the cause of the three unsteady features, because of the mismatch between k_{13}, the x-wavenumber that arises in the spurious free wave, and k_x, the x-wavenumber in the corresponding term of the third-order wave solution. For a travelling wave of permanent form, every term in the expansion must be bound to the first-order term as a higher harmonic of that term. (Sometimes the harmonics are called 'bound waves'.) So, the harmonic term with the wave vector $(k_x, 3k_y)$ does not satisfy the linearized dispersion relation (3) with frequency ω, and it travels at the speed of the first-order term. But the spurious free wave with wave vector $(k_{13}, 3k_y)$ does satisfy the linear dispersion relation (4) with frequency ω and travels at a corresponding free-wave speed. So, the spurious free wave travels at a different speed and is not bound to the first-order solution. The difference between k_{13} and k_x causes the modulation or 'beat' of the wavetrains in the x-direction. This beat is the first unsteady feature listed in §1. In their (4.14), FM predict the beat length to be

$$L_B = L_x \frac{\sin \theta}{\sin \theta - \sqrt{1 - 9 \cos^2 \theta}}, \quad (7)$$

where $L_x = 2\pi/k_x$. They also predict the beat amplitude to be

$$a_B = \frac{a^3 k^2}{2} |b_{13}| \quad (8)$$

where b_{13} is given by (5.1) of FM.

The second unsteady feature listed in §1 is the curving of crestlines, which can be seen in figure 5(a), below. FM explained this observed curving of crestlines as being due to the phase of the spurious b_{13}-term in (6) relative to the corresponding bound b_{13}-term in (5): "If the peak of the spurious free wave at a given location is slightly in front of or behind a primary wave crest, it will respectively appear to bend it frontwards or backwards." FM stated that the third unsteady feature, dips and peaks in the crestlines in the y-direction, also occurs when the spurious free b_{13}-term and the bound b_{13}-term are out of phase.

HHS derived coupled nonlinear Schrödinger equations to describe their experiments. They computed the surface displacement to third order, based on the exact solution of the coupled nonlinear Schrödinger equations that yields (2). Their computations of the surface displacements, which had third-order terms corresponding to (5), accounted for a slight curving of crest lines and for dips and peaks in the crest lines. However, FM rightly point out that when the amplitude is large enough so that the third-order solution exhibits such features, then one has not carried the expansion out to high enough orders for it to be applicable to the physical problem. For example, large-amplitude solutions from a 27th-order expansion (Roberts 1983) do not exhibit such features. See FM for additional references that discuss this point. HHS also discussed instability of the exact solution as being a potential explanation for their observed unsteadiness. The stability of wavefields produced by obliquely interacting wavetrains is examined, for example, by Ioualalen & Kharif (1994), who classified instability regimes based on wave steepness, Kimmoun, Ioualalen & Kharif (1999*b*), who extended their work, and others listed in these references. Nevertheless, FM pointed out that the unsteadiness observed in the experiments of HHS occurred directly off the paddle; it did not grow on the time scales predicted by these stability analyses.

3. Wavemaker considerations

The theory outlined above introduces one consideration when generating periodic wavetrains of permanent form in a laboratory. Several additional considerations arise from the presence of the time-dependent boundary at the wavemaker, and the finite length and width of the wave basin. These considerations comprise 'the wavemaker problem', in which one determines the wavemaker motion that results in a desired waveform. A variety of mechanical wavemakers are used in laboratories: piston-type wavemakers (that move horizontally) are typically used for waves in shallow water; plungers (that move vertically) and flaps are typically used for waves in deep water.

Linearized theories that include a boundary due to the wavemaker provide predictions of wave amplitude radiating away from the wavemaker, the shape of the evanescent modes trapped at the wavemaker for a given wavemaker amplitude, and the power required by particular wavemaker geometries. Linearized wavemaker theory is presented, for example, by Dean & Dalrymple (1984, especially pp. 170–186). Experimental confirmation of far-field wave amplitude predictions is provided, for example, by Ursell, Dean & Yu (1960), Galvin (1964, as referenced by Sulisz & Hudspeth, 1993), Keating & Weber (1977), Patel & Ioannou (1980), Hudspeth, Leonard, & Chen (1981), and Henderson & Lee (1986) for piston and flap-type wavemakers.

Plunger-type wavemakers, like those used herein and in HHS, are more difficult to treat analytically because, unless they are very thin or very wide, the domain that includes them is not separable with respect to the horizontal and vertical dimensions, even in the linearized problem. Wang (1974) and Wu (1988, 1991) solved approximate linear problems numerically. Experiments were conducted by Wang (1974), Patel & Ioannou (1980), Ellix & Arumugam (1984), and Pritt (2003). Ellix & Arumugam found that leakage behind the wavemaker, the superharmonic component of the waves, and reflections from the beach needed to be considered in their comparisons with theory. Pritt, who used a triangular plunger with the same controller as used by HHS and by us, found that agreement with theory depended on whether the wave frequencies were below or above 5 Hz where surface tension effects became important,

and whether experiments below 5 Hz were conducted on 'dirty' or 'clean' water so that viscous effects were or were not important.

All of this work is for wavemakers that produce plane waves. Segmented wavemakers can be used to generate waves with two-dimensional surface patterns. (See figure 1 for both a segmented wavemaker array, and the surface pattern created by it.) These wavemakers involve additional considerations, even in the linearized problem. For example, Gilbert (1976, as quoted by Schäffer & Steenberg 2003) found that spurious modes were generated due to the finite segment widths.

The nonlinear wavemaker problem involves finding a prescribed paddle motion of finite amplitude that produces a desired wavefield, also of finite amplitude. The second-order theory was developed first by Fontanet (1961, as referenced by Sulisz & Hudspeth, 1993). See Schäffer (1996) and Schäffer & Steenberg (2003) for literature reviews. Several issues arise when considering nonlinear effects. The primary one is to obtain a proper wavemaker forcing that suppresses spurious harmonic modes. There has been much work on this problem. An example of experimental confirmation is in Schäffer (1996), who showed time series obtained from experiments using first- and second-order forcing signals, derived in the same paper, to generate waves with a piston wavemaker that propagated in one horizontal dimension. His results show the suppression of spurious second-harmonics by the nonlinear forcing, for monochromatic waves, for wave groups, and for irregular wavefields (multi-frequency wavefields) corresponding to JONSWAP spectra. In addition to the suppression of spurious modes, other nonlinear wavemaker issues include: the effects of the first-order evanescent wavefield on the second-order solution (e.g. Sulisz & Hudspeth 1993); Stokes drift and return flows in wave flumes (e.g. Hudspeth & Sulisz 1991 and Sulisz & Hudspeth 1993); the effects of sidewall reflections (e.g. Li & Williams 1998); sum and difference interactions among generated waves with different frequencies (e.g. Moubayed & Williams 1994 and Schäffer 1996); and mechanical wave absorption of unwanted radiated waves (e.g. Schäffer 1998). Schäffer & Steenberg (2003) generalized the work of Schäffer (1996) to obtain second-order motions for piston and flap-type wavepaddles that can generate multidirectional, irregular wavefields. FM considered the effects of spurious modes generated by neglecting third-order terms in the wavemaker forcing (in the absence of the boundary due to a particular wavemaker geometry). As discussed in §2, they showed that for waves with two-dimensional surface patterns, the consequences of neglecting third-order terms are even more pronounced than those of neglecting the second-order terms.

The success of any forcing function in producing a desired waveform depends on the quality of control provided to the wavemaker. Mechanical systems have their own nonlinearities, and may therefore input their own harmonics, which would appear as additional spurious free waves in the wavefield. Flick & Guza (1980) discuss this point.

In some experiments, the desired waveform is an exact solution to a nonlinear evolution equation. Such solutions necessarily include higher harmonics in their descriptions. Goring & Raichlen (1980) found that they could produce clean cnoidal waves (as periodic solutions to the KdV equation) with a piston wavemaker by programming the wavemaker with the cnoidal wave solution and accounting for the finite displacement of the wavemaker. This procedure was used by Hammack *et al.* (2004) to generate clean solitons as localized solutions of the KdV equation using a piston wavemaker. Hammack, Scheffner & Segur (1989) attempted to use the procedure to generate bi-periodic patterns of waves in shallow water. They programmed their 60-piston wavemaker array with the genus-2 solutions of the KP equation, taking into account the finite displacement of the wavemakers. However,

they reported that cleaner patterns resulted from the oblique interaction of cnoidal waves instead. Nevertheless, their measurements of the resulting patterns agreed well with the KP solution.

Previous experiments on deep-water waves using plungers with triangular and exponential cross-sections did not seem to suffer from the contamination of spurious modes due to the neglect of second-order harmonics. In particular Segur *et al.* (2005) conducted experiments with such wavemakers using monochromatic wavetrains with and without modulations (two nearby sideband modes). They did not account for spurious harmonics, but observed very good agreement, with no free parameters, between Fourier amplitudes obtained from measured time series, including the amplitude of the second harmonic, and predictions from nonlinear theories. In contrast, earlier deep-water experiments by Lake & Yuen (1977) measured second-harmonic amplitudes that did not agree with the prediction from Stokes expansion.

Segur *et al.* (2005) found that dissipative effects must be incorporated into the nonlinear Schrödinger model for the evolution of deep-water waves to predict, both qualitatively and quantitatively, measured wave evolutions. Henderson & Lee (1986) and Pritt (2003) found that comparisons of measurements of far-field amplitudes with prediction from the linear wavemaker problem were affected by the 'cleanliness' of the water. So, damping is also a consideration in designing a wavemaker motion to produce a desired waveform. Damping is particularly important in the 4 Hz motions used in the HHS experiments and those herein. Viscous effects have been included in numerical wave tanks, for example by Park *et al.* (2004) and references listed therein, who integrated the Navier–Stokes equations and allowed for fully nonlinear multi-directional waves.

In this section, we have discussed briefly some of the issues that arise when attempting to generate a desired waveform with a mechanical wavemaker. The spurious free modes caused by neglecting harmonics in the wavemaker forcing are an important issue. Suprisingly, FM found that third-harmonic terms are more important than second-harmonic terms when the wavefields have two-dimensional surface patterns. The spurious modes are present regardless of the wavemaker geometry; however, knowing how to control the wavemaker to suppress them means solving the nonlinear wavemaker problem for the particular wavemaker geometry. HHS and we use a plunger-type wavemaker array for which neither the linearized nor the nonlinear theory has been worked out. The effects of the interactions between first-order evanescent fields generated by each wave and their interactions with the second and third harmonics of the wavefields are not known. The wavemaker array is segmented, a situation that can introduce additional spurious free modes that were not accounted for in FM's work. The parameter regime of the experiments is such that dissipative effects are important. Nevertheless, in the remainder of the paper, we report on experiments that consider only the issue of spurious free modes resulting from the neglect of third-harmonic terms, as discussed by FM, and find that by including them, we can generate waves with two-dimensional surface patterns that propagate with nearly permanent form in deep water.

4. Experiments

Experiments to test the predictions of FM were conducted in the tank used by HHS, shown in figure 1: a wave basin that is 12 ft long, $W = 6$ ft wide, and 1 ft deep with an undisturbed water depth of $h = 20$ cm. Along one 6 ft endwall is a segmented wavemaker comprising 32 side-by-side, vertically oscillating triangular wedges (paddles)

that intersect the water surface. The motion of each paddle is independently programmable and controlled so that the segmented wavemaker can generate complex wavefields comprising multiple waves propagating at arbitrary angles. (Details of the apparatus are presented in HHS.)

HHS generated two-dimensional surface patterns using one or the other of two types of forcings. For the one corresponding to (2), the vertical displacement of the jth paddle with $1 \leqslant j \leqslant 32$ was given by

$$Z_j = a^p \cos(k_y y_j) \cos(\omega t), \tag{9}$$

with y_j corresponding to the y-location of the middle of the jth paddle. The velocities of the wavepaddles were obtained by using a similarly digitized version of the time-derivative of (9). This forcing function produced the photograph shown in figure 1. Here, a^p is the amplitude of the paddles' oscillations, not those of the water wave. We note that no x-wavenumber or x-dependence is shown in (9). We control frequency only; wave dynamics determines wavenumbers.

To test the prediction by FM, we programmed the wavemaker according to (9), and then compared the results of those experiments with other experiments in which we modified the wavemaker forcing function. The modification included a term like the b_{13}-term in (5), identified by FM as the term whose neglect caused the three unsteady features. So in the modified experiments, we forced the paddle according to

$$Z_j = a^p \cos(k_y y_j) \cos(\omega t) + a_3{}^p \cos(3k_y y_j) \cos(\omega t), \tag{10}$$

with the velocities of the wave paddles obtained by using a similarly digitized version of the time-derivative of (10). We note that the additional term, which is one of the third harmonics of the fundamental, has the same frequency as the fundamental; it is a third harmonic in its y-spatial dependence.

The experimental procedure was as follows. We cleaned the tank with alcohol and filled it with tap water to a depth greater than 20 cm. Before each set of experiments, we cleaned the air–water interface using a piece of brass angle that spans the tank in the y-direction. It is mounted on bearings that roll along fixed railings on each 12 ft side of the tank. The brass angle is parallel to the wave paddles and was lowered until it intersected the water surface. We rolled the brass angle down the tank in the x-direction, scraping the surface and any film or particles on it to the end of the tank. We vacuumed the surface at the end using a wet-vac. Then we rolled the brass angle back to the paddles and vacuumed the surface in that region until the depth of water was 20 cm. Then we lifted the brass angle away from the surface. We conducted experiments within a 2 hour period after cleaning the surface. (Segur *et al.* 2005 showed that the rate of wave damping remains approximately constant for about 2 hours). Then we added water, cleaned the surface again and conducted more experiments in another 2 hour period. In this way, we used the same water for days, but always started with a 'clean' surface. This procedure allowed reproducible results.

We generated wave patterns using either (9) or (10). We measured wavefields using capacitance-type wave gauges supported above the basin on a carriage that moved in the x-direction to investigate the beats that arise in x (the direction of propagation), or in the (negative) y-direction to investigate the dips and peaks that occur on crestlines (approximately) parallel to the paddle array. The carriage speed was constant, typically in the range of 7–10 cm s^{-1} during traverses in the x-direction, with variations due to the experimental parameters; it was 4.0 cm s^{-1} during traverses in the y-direction. Each wave gauge measured the instantaneous water-surface displacement at a 'point' (a circular area of about 1 mm diameter).

Gauge number	x (cm)	y (cm)
gauge_{1x}	46.3	61.0
gauge_{2x}	46.3	121.8
gauge_{3x}	46.3	91.4
gauge_{4x}	29.0	91.4
gauge_{1y}	29.5	153.9
gauge_{2y}	48.5	153.9
gauge_{3y}	86.5	153.9

TABLE 1. Initial location of the gauges with $(x, y) = (0, 0)$ as shown in figure 1.

For the experiments in which we investigated beat lengths, there were four gauges available, which we call 'gauge_{mx}' with $m = 1, 2, 3, 4$. Their initial positions in the wavetank, relative to the coordinate system shown in figure 1, are given in table 1. Two of the gauges ($3x$ and $4x$) were in nodal lines during experiments with an odd number of nodal lines in the tank. For the experiments in which we investigated dips and peaks along the crestlines, three gauges were available, which we call 'gauge_{my}' with $m = 1, 2, 3$. We also used this gauge configuration for the experiment in figure 2. Their initial positions are also listed in table 1.

5. Results

In this section we compare our measurements with the predictions of FM. In particular, we discuss five features of the wave patterns. FM predicted (i) the existence of beats in the wavefields along an axis parallel to the x-axis, and how to program the wavemakers to generate wavetrains with no beats. They further predicted (ii) the beat lengths and (iii) the beat amplitudes. FM predicted the existence of both (iv) curved crestlines and (v) dips and peaks in the crestlines along an axis parallel to the y-axis, as well as how to program the wavemakers to remove them. In this section we verify (i), (ii), (iv), (v), and find some disagreement between measurements and predictions for (iii). These are our main results.

5.1. *Beats*

The infinite series in (1) that represents a travelling wave pattern of permanent form and that has a first-order term given by (2) has oscillations in x with an amplitude that is constant in x. HHS showed, by traversing a measuring gauge through the wave pattern in the x-direction, that the wave envelope exhibited a slow modulation, or 'beat', on the amplitudes of the oscillation in that direction. Our experiments exhibit the same behaviour; figure 2 shows time series from gauge_{1y} in three experiments as it traversed in the x-direction at a speed of $v = 9.22\,\text{cm s}^{-1}$. The carriage began moving a few seconds after the waves reached the gauges, so there is a Doppler shift in the signal near the beginning of the time series. At about 23 s, the waves that had reflected off the back wall of the tank reached the gauges. These constraints gave us about a 200 cm interval in x in which to observe the beats.

Figure 2(a) is obtained from an experiment using the forcing of (9). A beat is evident in the time series, directly off the paddles. Figures 2(b) and 2(c) are obtained from second and third experiments using the forcing of (10). The presence of the b_{13}-type term in the forcing decreased the beat amplitude as shown in figure 2(b). An increase in the magnitude of the b_{13}-term caused the beat to essentially disappear, as shown in figure 2(c). A further increase in the magnitude of the b_{13}-term caused the
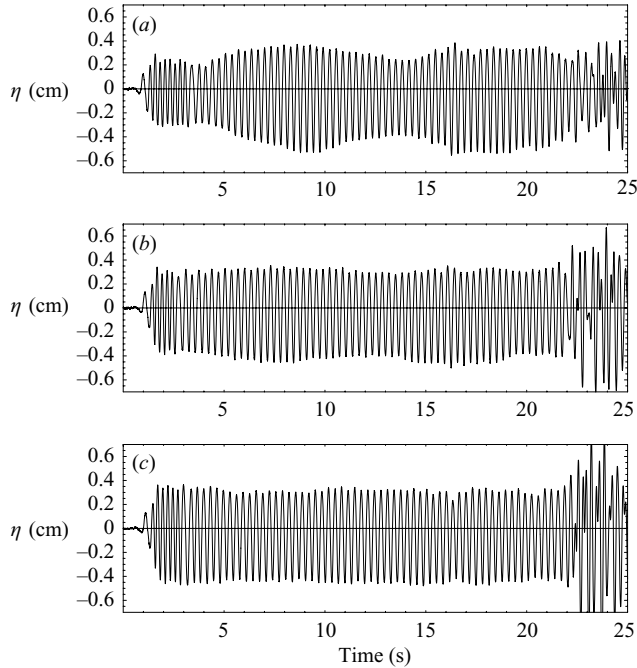
FIGURE 2. Time series of a 4 Hz pattern with $\omega = 4(2\pi)\,\text{s}^{-1}$, $\theta = 82.1°$, $n = 5$. (a) $a^p = 0.80\,\text{cm}$, $a_3{}^p = 0\,\text{cm}$. (b) $a^p = 0.80\,\text{cm}$, $a_3{}^p = -0.10\,\text{cm}$. (c) $a^p = 0.80\,\text{cm}$, $a_3{}^p = -0.20\,\text{cm}$.

beat to reappear (not shown). In general, to determine the forcing amplitude of the b_{13} term, $a_3{}^p$, that corresponds to the predicted beat amplitude, we did the following.

(i) We chose a^p. In the experiment that does not include the b_{13}-type term in the forcing, we found the resulting water wave amplitude, a, of the 4 Hz wave, obtained from a Fourier transform of the time series.

(ii) Using a from (i) and b_{13} from (5.1) of FM, we used (8) to compute the beat amplitude, a_B, generated by the b_{13} term in (5).

(iii) The b_{13}-type term has the same paddle oscillation frequency as the fundamental. So, using (i) and (ii) we can extrapolate a 'predicted' forcing amplitude of the b_{13} term to be

$$a_3{}^p = a_B a^p \, \text{sgn}(b_{13})/a. \tag{11}$$

For the experiments shown in figure 2, $a^p = 0.80\,\text{cm}$, $a = 0.39\,\text{cm}$ and $a_B = 0.08\,\text{cm}$, so that $a_3{}^p = -0.16\,\text{cm}$. This 'predicted' value lies between the two used in figures 2(b) and 2(c).

From time series such as those in figure 2, we measured the beat length L_B and beat amplitude a_B as a function of mode number n, or correspondingly, angle θ, (3), of the two interacting waves. First, we estimated the values by eye directly from the time series. Second, we employed a multi-resolution wavelet analysis of the envelope of the data to obtain more objective measures for the beat lengths. It consisted of (i) obtaining the envelope of the time series by extracting the maximum excursions of the water surface during each carrier-wave period; (ii) decomposing the envelope via a Daubechies discrete wavelet transform (db5) (see, for example, Mallet 1999); (iii) reconstructing an approximate envelope from the coefficients that corresponded to the length scale of the beat that was visible to the eye; (iv) computing a Fourier transform of this approximate envelope. The beat length corresponded to the
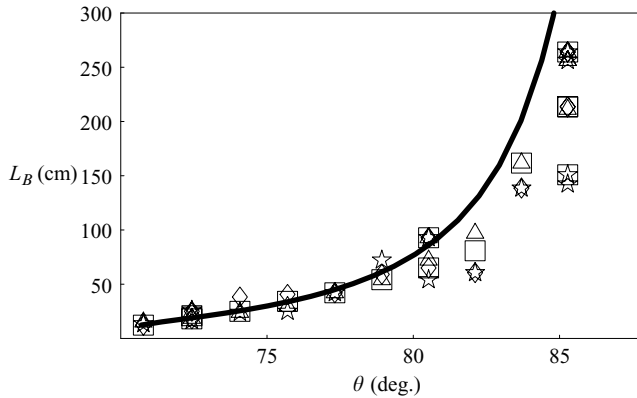
FIGURE 3. Prediction and measurements of beat lengths. The prediction (curve) is from (7). Measurements are from gauge$_{1x}$ (triangles); gauge$_{2x}$ (squares); gauge$_{3x}$ (stars); gauge$_{4x}$ (diamonds).

periodicity with the peak of that transform. Third, the beat amplitudes were acquired by assuming the time series was a sum of the carrier wave and a beat. A MATLAB optimization routine then returned a beat amplitude that minimized the difference between the measured time series and the assumed time series. The results for both beat length and beat amplitude were consistent with our initial 'by eye' estimates.

Figure 3 shows the results for beat length. The agreement between measurements and predictions from (7) is good for angles below about 82°. For higher angles (7) overestimates the observed beat length. FM found very good agreement between (7) and results from their numerical simulations of a dispersive Boussinesq system of equations, and also found that (7) overestimated L_B at higher angles. They could obtain better agreement at higher angles by decreasing the wave amplitude. We looked for an amplitude dependence on beat length for the $n = 7, \theta = 78.9°$ case and for the $n = 4, \theta = 83.7°$ case, but did not observe one. For our experiments, the measurement interval was comparable to or shorter than the predicted beat length for angles θ exceeding about 83°, so it was difficult to resolve a beat length for these experiments. Further, FM warn that disagreement for $\theta \to \pi/2$ is perhaps expected, since the perturbation solution has a zero radius of convergence in that limit.

Figure 4 shows the results for the beat amplitude. The solid points are from predictions using (8) and the measured values of a for the particular experiment. The hollow symbols are measurements from two gauges as indicated. Here the predictions generally underestimated the measured beat amplitudes. The discrepancy is likely to be due to the difference in boundary conditions at the wavemaker from the numerical simulations of FM and the plunger array used in the experiments (see §3).

5.2. *Curved crestlines*

The infinite series in (1) that represents a travelling wave pattern of permanent form and that has a first-order term given by (2) has crestlines parallel to the y-axis with no curvature in the horizontal. Crestlines in the experiments of HHS did exhibit curvature in the horizontal, and FM explained this non-uniformity with the b_{13}-type term. An example from our experiments is shown in figure 5, which is photographs of the bottom of the wavetank during two experiments. One can see a large-scale pattern, the wavefield under consideration here, and waves with a smaller length scale superposed. The waves propagated from right to left. The bright lines in the page's
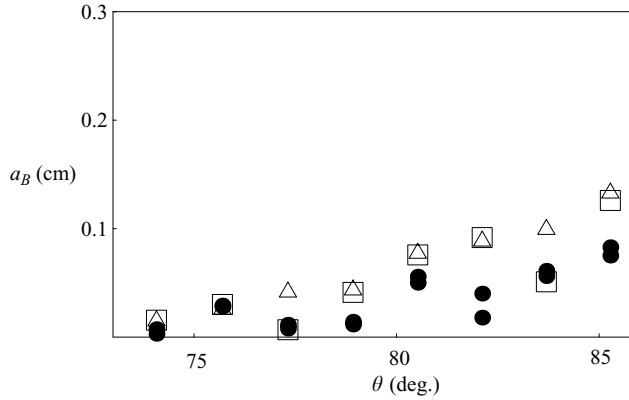
FIGURE 4. Predictions (solid circles) and measurements of beat amplitudes. Measurements are from gauge$_{1x}$ (triangles) and gauge$_{2x}$ (squares).
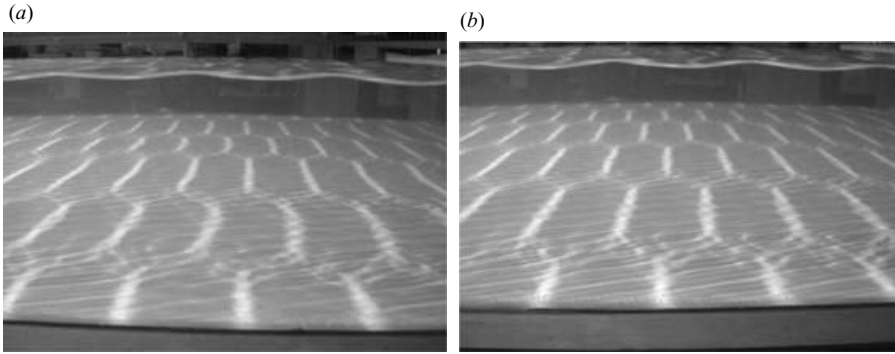

FIGURE 5. Photograph of the bottom of the tank showing crest lines for a 4 Hz pattern with $\omega = 4(2\pi)\,\mathrm{s}^{-1}$, $\theta = 82.1°$, $n = 5$. (*a*) $a^p = 0.40\,\mathrm{cm}$, $a_3{}^p = 0\,\mathrm{cm}$. (*b*) $a^p = 0.40\,\mathrm{cm}$, $a_3{}^p = -0.05\,\mathrm{cm}$.

vertical direction, approximately parallel to the wavemaker array, correspond to the crestlines at the water surface, which is visible at the top of the pictures.

Figure 5(*a*) is from an experiment in which the wavemaker forcing corresponded to (9). The crestlines exhibited a non-uniform curvature similar to those from numerical computations that FM showed in their figure 2. Figure 5(*b*) is from an experiment in which the wavemaker forcing corresponded to (10). The crestlines are straight. For this experiment, $a^p = 0.40\,\mathrm{cm}$ and $a = 0.21\,\mathrm{cm}$, so that $a_B = 0.012\,\mathrm{cm}$. Using (11) we compute the prediction $a_3{}^p = -0.02\,\mathrm{cm}$. In figure 5(*b*) we used $a_3{}^p = -0.05\,\mathrm{cm}$. (We did not do an experiment with $a_3{}^p = -0.02\,\mathrm{cm}$.) So, the presence of a b_{13}-type term made the wavefield more nearly uniform than it was without that term, as predicted by FM.

5.3. *Dips and peaks along crestlines*

The infinite series in (1) that represents a travelling wave pattern of permanent form and that has a first-order term given by (2) has crestlines with a single maximum in each period in the *y*-direction. The experiments of HHS gave measurements of crestlines with dips in the middle and peaks near the nodal lines of each period. FM explained these dips and peaks with the b_{13}-type term. An example from our experiments is presented in figure 6, which shows time series obtained from three
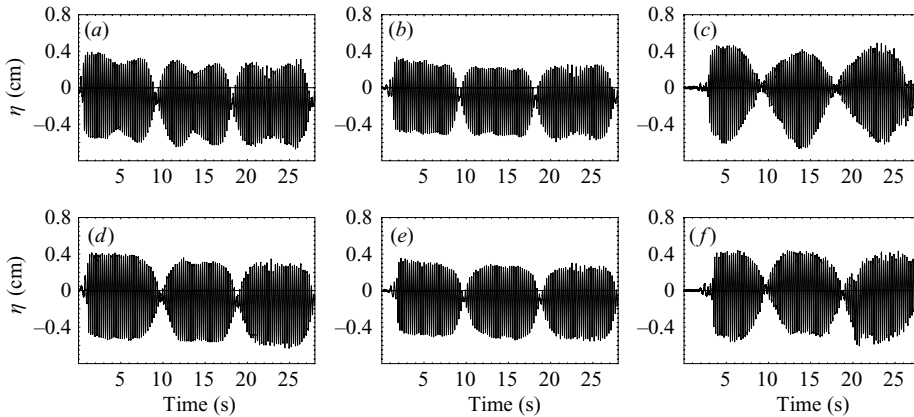
FIGURE 6. Time series from three gauges for a $4\,\mathrm{Hz}$ pattern with $\omega = 4(2\pi)\,\mathrm{s}^{-1}$, $\theta = 82.1°$, $n = 5$. (a) Gauge$_{1y}$, (b) gauge$_{2y}$, (c) gauge$_{3y}$: $a^p = 0.80\,\mathrm{cm}$; $a_3{}^p = 0$. (d) Gauge$_{1y}$, (e) gauge$_{2y}$, (f) gauge$_{3y}$: $a^p = 0.80\,\mathrm{cm}$; $a_3{}^p = -0.15\,\mathrm{cm}$.

gauges (gauge$_{my}$, $m = 1, 2, 3$) in two experiments in which the gauges traversed the tank in the y-direction. The gauge locations are listed in table 1.

In the experiment shown in figure 6(a–c), the b_{13}-type term was not included in the wavemaker forcing. This experiment used the same parameters as that shown in figure 2(a), and resulted in a wave amplitude of $a = 0.38\,\mathrm{cm}$. Gauge$_{1y}$ (with $x = 29.5\,\mathrm{cm}$) measured a y-variation of the crestlines characterized by dips in each antinodal region with corresponding peaks near the nodal regions. Gauge$_{2y}$ (with $x = 48.5\,\mathrm{cm}$) measured a similar time series with a less pronounced arrangement of dips and peaks. Gauge$_{3y}$ (with $x = 86.5\,\mathrm{cm}$) measured a time series that did not have dips and peaks, but had an asymmetric cosine variation in the y-direction. So, the pattern had a y-structure that is not present in the infinite series representation in (1). Further, this structure varied with x, in contrast to the infinite series representation.

In the experiment shown in figure 6(d–f) the b_{13}-type term was included in the wavemaker forcing. The dips and peaks did not disappear, but the resulting time series from the gauge-traverse in the y-direction had a wave amplitude that was much nearer to constant in the y-direction. In addition, the variation at the different x-locations of the three gauge sites was significantly reduced. So, the inclusion of the b_{13}-type term resulted in a nearer to permanent-form solution. FM explained the remaining dips and peaks as the effects of even higher-order harmonics not included in the wavemaker forcing. In the experiment of figure 6(a–c), $a^p = 0.80\,\mathrm{cm}$ and $a = 0.38\,\mathrm{cm}$, so that $a_B = 0.012\,\mathrm{cm}$. Using (11), we obtain a predicted $a_3{}^p = -0.15\,\mathrm{cm}$. This is the value that we used in the experiment of figure 6(d–f).

REFERENCES

BADULIN, S. I., SHRIRA, V. I., KHARIF, C. & IOUALALEN, M. 1995 On two approaches to the problem of instability of short-crested water waves. *J. Fluid Mech.* **303**, 297–326.

BRYANT, P. J. 1985 Doubly periodic progressive permanent waves in deep water. *J. Fluid Mech.* **161**, 27–42.

CAULLIEZ, G. & COLLARD, F. 1999 Three-dimensional evolution of wind waves from gravity-capillary to short gravity range. *Eur. J. Mech.* B **18**, 389–402.

CAULLIEZ, F., RICCI, N. & DUPONT, R. 1998 The generation of the first visible wind waves. *Phys. Fluids* **10**, 757–759.

COLLARD, F. & CAULLIEZ, G. 1999 Oscillating crescent-shaped water wave patterns. *Phys. Fluids* **11**, 3195–3197.

DEAN, R. G. & DALRYMPLE, R. A. 1984 *Water Wave Mechanics for Engineers and Scientists.* Prentice Hall.

ELLIX, D. & ARUMUGAM, K. 1984 An experimental study of waves generated by an oscillating wedge. *J. Hydraul. Res.* **22**, 229–313.

FLICK, R. E. & GUZA, R. T. 1980 Paddle generated waves in laboratory channels. *J. Waterway, Port, Coastal Ocean Div., WW1, ASCE* **106**, 79–97.

FONTANET, P. 1961 Theórie de la génération de la houle cylindrique par un batteur plan. *La Houille Blanche* **16**, 3–31.

FUHRMAN, D. R. & MADSEN, P. A. 2006 Short-crested waves in deep water: A numerical investigation of recent laboratory experiments. *J. Fluid Mech.* **559**, 391–411 (referred to herein as FM).

GALVIN, C. J. 1964 Wave-height prediction for wave generators in shallow water. *Tech. Mem.* 4, pp. 1–20. US Army Corps of Engineers, Washington, DC, USA.

GILBERT, G. 1976 Generation of oblique waves. *Tech.l Rep. 18.* Hydraulic Research Station, Wallingford, UK.

GORING, D. G. & RAICHLEN, F. 1980 The generation of long waves in the laboratory. *Proc. 17th Intl Conf. Coastal Engrs, Sydney, Australia.*

HAMMACK, J. & HENDERSON, D. 2003 Experiments on deep-water waves with two-dimensional surface patterns. *J. Offshore Mech. Arctic Engng Special issue: J. V. Wehausen Symposium on Water Waves, Ship Waves, and Marine Hydrodynamics* **125**, 48–53.

HAMMACK, J. L., HENDERSON, D. M., GUYENNE, P. & YI, M. 2004 Solitary-wave collisions. *Proc. ASME Offshore Mechanics and Arctic Engineering: A Symposium to Honor Theodore Yao-Tsu Wu.* World Scientific.

HAMMACK, J. L., HENDERSON, D. M. & SEGUR, H. 2005 Progressive waves with persistent two-dimensional surface patterns in deep water. *J. Fluid Mech.* **532**, 1–52 (referred to herein as HHS).

HAMMACK, J., SCHEFFNER, N. & SEGUR, H. 1989 Two-dimensional periodic waves in shallow water. *J. Fluid Mech.* **209**, 567–589.

HENDERSON, D. M. & LEE, R. C. 1986 Laboratory generation and propagation of ripples. *Phys. Fluids* **29**, 619–624.

HSU, J. R., TSUCHIYA, Y. & SILVESTER, R. 1979 Third-order approximation to short-crested waves. *J. Fluid Mech.* **90**, 179–196.

HUDSPETH, R. T., LEONARD, J. W. & CHEN, M.-C. 1981 Design curves for hinged wavemakers: Experiment. *J. Hydraul. Div. ASCE* **107**, 553–574.

HUDSPETH, R. T. & SULISZ, W. 1991 Stokes drift in two-dimensional wave flumes. *J. Fluid Mech.* **230**, 209–229.

IOUALALEN, M. 1993 Fourth order approximation of short–crested waves. *C. R. Acad. Sci. Paris* II **316**, 1193–1200.

IOUALALEN, M. & KHARIF, C. 1994 On the subharmonic instabilities of steady three-dimensional deep water waves. *J. Fluid Mech.* **262**, 265–291.

KEATING, T. & WEBER, N. B. 1977 The generation of periodic waves in a laboratory channel: a comparison of theory and experiment. *Proc. Inst. Civil Engrs* **63**, 819–832.

KIMMOUN, O., BRANGER, H. & KHARIF, C. 1999a On short-crested waves: Experimental and analytical investigations. *Eur. J. Mech.* B **18**, 889–930.

KIMMOUN, O., IOUALALEN, M. & KHARIF, C. 1999b Instabilities of steep shortcrested surface waves in deep water. *Phys. Fluids* **11**, 1679–1681.

LAKE, B. M. & YUEN, H. C. 1977 A note on some water–wave experiments and the comparison of data with theory. *J. Fluid Mech.* **83**, 75–81.

LI, W. & WILLIAMS, A. 1998 Second-order three-dimensional wavemaker theory with side-wall reflection. *Proc. 8th Intl Offshore and Polar Engng Conf. Montreal Canada*, pp. 235–241.

MALLET S. 1999 *A Wavelet Tour of Signal Processing*. Academic.

MOUBAYED, W. I. & WILLIAMS, A. N. 1994 Second-order bichromatic waves produced by a generic planar wavemaker in a two-dimensional wave flume. *J. Fluid Struc.* **8**, 73–92.

PARK, J. C., UNO, Y., SATO, T., MIYATA, H. & CHUN, H. H. 2004 Numerical reproduction of fully nonlinear multi-directional waves by a viscous 3D numerical wave tank. *Ocean Engng* **31**, 1549–1565.

PATEL, N. H. & IOANNOU, P. A. 1980 Comparative performance study of paddle- and wedge-type wave generators. *J. Hydraul.* **14**, 5–9.

PRITT, T. D. 2003 Linear wavemaker problem for triangular and exponentially shaped wavemakers. MA.Thesis, Penn State University.

ROBERTS, A. J. 1983 Highly nonlinear short-crested water waves. *J. Fluid Mech.* **135**, 301–321.

ROBERTS, A. J. & PEREGRINE, D. H. 1983 Notes on long-crested water waves. *J. Fluid Mech.* **135**, 323–335.

ROBERTS, A. J. & SCHWARZ, L. W. 1983 The calculation of nonlinear short-crested gravity waves. *Phys. Fluids* **26**, 2388–2392.

SCHÄFFER, H. A. 1996 Second-order wavemaker theory for irregular waves. *Ocean Engng* **23**, 47–88.

SCHÄFFER, H. A. 1998 Some design aspects of an absorbing 3D wavemaker. *Proc. 26th Intl Conf. Coastal Engng* **1**, 1082–1095.

SCHÄFFER, H. A. & STEENBERG, C. M. 2003 Second-order wavemaker theory for multidirectional waves. *Ocean Engng* **30**, 1203–1231.

SEGUR, H., HENDERSON, D., CARTER, J., HAMMACK, J., LI, C.-M., PHEIFF, D. & SOCHA, K. 2005 Stabilizing the Benjamin-Feir instability. *J. Fluid Mech.* **539**, 229–271.

SU, M.-Y. 1982 Three-dimensional deep-water waves. Part 1. Experimental measurement of skew and symmetric wave patterns. *J. Fluid Mech.* **124**, 73–108.

SU, M.-Y., BERGIN, M., MARLER, P. & MYRICK, R. 1982 Experiments on nonlinear instabilities and evolution of steep gravity-wave trains. *J. Fluid Mech.* **124**, 45–72.

SULISZ, W. & HUDSPETH, R. T. 1993 Complete second-order solution for water waves generated in wave flumes, *J. Fluids Struct.* **7**, 253–268.

URSELL, F., DEAN, R. G. & YU, Y. S. 1960 Forced small–amplitude water waves: a comparison of theory and experiment. *J. Fluid Mech.* **7**, 33–52.

WANG, S. 1974 Plunger-type wavemakers: theory and experiment. *J. Hydraul. Res.* **12**, 357–387.

WU, Y.-C. 1988 Plunger-type wavemaker theory. *J. Hydraul. Res.* **26**, 483–491.

WU, Y.-C. 1991 Waves generated by a plunger-type wavemaker. *J. Hydraul. Res.* **29**, 851–860.